Morphology Studies of Multilayered HDPE/PS Systems

T. E. Bernal-Lara,[1] R. Masirek,[2] A. Hiltner,[1] E. Baer,[1] E. Piorkowska,[2] A. Galeski[2]

[1]*Department of Macromolecular Science and Engineering and Center for Applied Polymer Research, Case Western Reserve University, Cleveland, Ohio, 44106-7202*
[2]*Centre of Molecular and Macromolecular Studies, Polish Academy of Sciences, 90 363 Lodz, Poland*

Received 18 April 2005; accepted 4 May 2005
DOI 10.1002/app.22178
Published online in Wiley InterScience (www.interscience.wiley.com).

ABSTRACT: Films with alternating layers of high density polyethylene (HDPE) and polystyrene (PS) were prepared by layer-multiplying coextrusion, using two HDPEs differing in molecular weight. The crystal structure of extremely thin PE layers confined between PS layers was studied by small angle X-ray scattering (SAXS), wide angle X-ray diffraction (WAXS), and also by atomic force microscopy (AFM) and differential scanning calorimetry (DSC) technique including MDSC. The morphology of HDPE in the systems studied is greatly affected by the presence of HDPE/PS interfaces. In the HDPE layers, the texture component was observed with lamellae with their basal planes normal to the interface and (200) crystallographic planes parallel to the interface. Thus, the polymer chains in this texture component are parallel to the interface between both polymers. The small fraction of lamellae parallel to the interface in thicker HDPE layers disappears with the thinning of the layers beyond 100 nm. AFM images show in these samples straight, long lamellae positioned edge-on at HDPE/PS interface. The thickness and perfection of lamellae decrease with the decrease of individual HDPE layer thickness. Those thinner and less perfect lamellae are more susceptible to reorganization during heating as it is observed by MDSC. © 2005 Wiley Periodicals, Inc. J Appl Polym Sci 99: 597–612, 2006

Key words: polyethylene; microlayers; nanolayers; crystal texture; spatial confinement

INTRODUCTION

The role of nanostructured materials in various fields of technique continuously increases. A variety of methods were developed to manufacture metals and ceramics in a form of nanoparticles either separate or dispersed in another substance.

Micro- and nanolayers offer an opportunity to study the effect of reduced thickness and the influence of interface with foreign material on polymer crystallization. If the film thickness is less than the spherulite dimension, lamellae organize into flattened spherulites or "discoids."[1,2] Discoid lamellae are frequently oriented with respect to the surface. During crystallization of polyamide-6, the lamellae grow with hydrogen-bonded planes parallel to the film plane.[1] Discoids in poly(3-hydroxybutyrate) are composed of lamellae flat-on.[2] Polypropylene lamellae in thin films crystallize edge-on with macromolecular chains in the plane of the substrate.[3] Such orientation of chains was also reported for poly(ethylene naphthalate).[4] Further decrease of poly(ethylene terephthalate) film thickness results in replacement of discoids by crystals of other habit.[5] Recently, it was demonstrated that the orientation of isotactic polypropylene crystals depends strongly on interactions with a substrate.[6]

Many studies were focused on block copolymers, in which the crystalline domain constitutes one of the copolymer blocks.[7–13] Numerous block copolymer systems of different compositions, architectures, and morphologies were investigated.[14,15]

While the copolymer structure results from self-assembly, layer-multiplying coextrusion uses forced-assembly to create thousands of alternating layers of two polymers and allows to reduce an individual layer thickness below 10 nm.[16–18] Large number of layers permits the use of conventional methods of polymer analysis for studies of emerging structure.

Coextrusion of a crystallizable polymer as nanolayers confines the polymer chains to the size scale of the lamellar thickness. In the recent study,[19] thin isotactic polypropylene layers were coextruded between thick layers of amorphous polystyrene. In the layers thinner than 100 nm, in addition to a reduced crystallinity, a compressed *d*-spacing in the directions perpendicular to the chains and loss of registry along the chain axis were suggestive of smectic packing of conformationally distorted chains. Nevertheless, crystalline lamellae were still distinguishable in AFM images. In addition to the crystal population with (040) planes parallel to the interface, another crystal fraction was found

Correspondence to: E. Piorkowska (epiorkow@bilbo.cbmm.lodz.pl).

Contract grant sponsor: The State Committee for Scientific Research (Poland); contract grant number: 7 T08E 054 20.

TABLE I
Calculated LMHDPE Layer Thickness in LMHDPE Control Samples and in Multilayered LMHDPE/PS Films

LMHDPE/PS	Film thickness (μm)	Calculated LMHDPE layer thickness (nm)
100/0	266	—
100/0	137	—
100/0	40	—
90/10	270	890
90/10	135	950
90/10	40	270
70/30	280	1530
70/30	137	750
70/30	43	240
50/50	290	1140
50/50	173	680
50/50	48	190
30/70	262	610
30/70	140	330
30/70	25	60
20/80	312	490
20/80	142	220
20/80	48	80
10/90	297	230
10/90	147	110
10/90	46	35
05/95	48	19

with (110) planes parallel to the interface and (040) planes perpendicular to the interface, which possibly served to fill-in the radial structure of dendritic discoids when limited thickness of the layer left little space for secondary nucleation of cross-hatched lamella.

In polyethylene layers of thickness less than the dimensions of random coil of a polymer molecule, unique row-nucleated morphologies were found in the past.[20] Recent studies of high-density polyethylene (HDPE) nanolayers coextruded between thick layers of amorphous polystyrene[21] demonstrated that as the HDPE layers become thinner, the crystallinity decreased from 60 to 33%. Decreased crystallinity was accompanied by a change in morphology from banded spherulites to long bundles of edge-on lamella. The orientation of crystals was reflected also in 2D X-ray diffraction patterns, indicating that (200) plains become parallel to the film plane.

In the present study, the investigations are conducted for two HDPE/PS multilayered systems differing in molecular weight of HDPE. The varied crystallizable component content and thickness resulted in varying thickness of individual layers of HDPE. The attention is focused on detailed X-ray analysis of texture in micro- and nanolayers of the two HDPEs. Atomic force microscopy (AFM) together with conventional differential scanning calorimetry (DSC) and modulated differential scanning calorimetry (MDSC) were also used to study structure of HDPE in multilayered systems.

EXPERIMENTAL

The study utilized the two HDPEs: low molecular weight (LMHDPE), Quantum Petrothene, having M_w = 80 kg/mol and M_w/M_n = 3.75, and higher molecular weight (HMHDPE), Metallocene Dow C-MIX, having M_w = 125 kg/mol. Density of LMHDPE and HMHDPE was 0.954 and 0.9538 g/cm^3, respectively. Polystyrene (PS) was Dow STYRON 685D with bulk density 1.040 g/cm^3, according to ASTM D792. MFI of polymers studied, according to ASTM D1238, was 4.4 g/10 min for LMHDPE, 0.8 g/10 min for HMHDPE, and 1.5 g/10 min for PS.

Nanolayers of high density polyethylene (HDPE) and atactic polystyrene (PS), (HDPE/PS), with 257 layers were extruded from the melt on a laboratory scale coextrusion line at Case Western Reserve University that incorporates layer-multiplying technology. The total film thickness and relative composition were varied to produce polyethylene microlayers and nanolayers of different thickness. The weight composition of multilayered films was: 90/10, 70/30, 50/50, 30/70, 20/80, 10/90, and 5/95, while the total film thickness was in the range from 18 to approx. 300 μm; the deviation from the nominal total thickness did not exceed 2%. Thinner films were prepared by using a faster take-off speed. HDPE micro- and nanolayer having the nominal thickness from approx. 1500 to 7 nm were produced in this way. Control films of HDPE were coextruded in the same way. Nominal individual HDPE layer thickness in systems studied, calculated on the basis of total thickness and composition of multilayered film are presented in Tables I and II.

The thickness of selected individual HDPE and PS layers was measured by atomic force microscopy (AFM).[21] The film was embedded in epoxy (SPI-Chem™/SPI-PON™ 812 KIT formulation, SPI Supplies Division of Structure Probe, Inc.) and cured for

TABLE II
Calculated HMHDPE Layer Thickness in HMHDPE Control Samples and in Multilayered HMHDPE/PS Films

HMHDPE/PS	Film thickness (μm)	Calculated HMHDPE layer thickness (nm)
100/0	305	—
100/0	51	—
50/50	279	1100
50/50	47	180
30/70	48	110
10/90	305	240
10/90	152	120
10/90	51	40
10/90	35	30
10/90	18	14
5/95	51	20
5/95	35	14
5/95	18	7

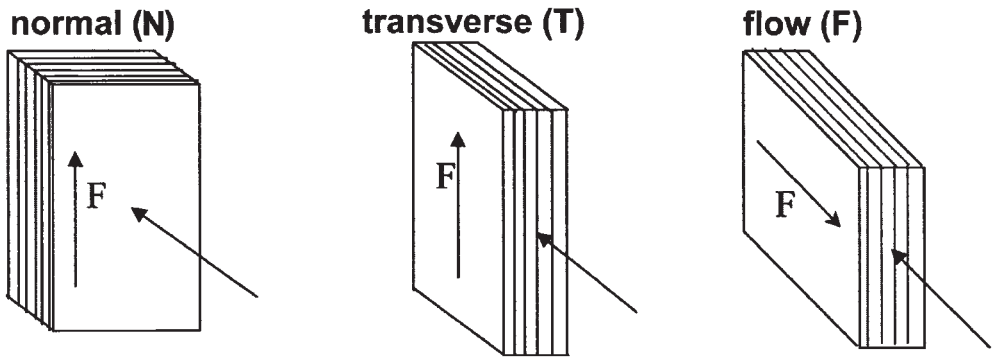

Figure 1 Scheme of the positions of the sample in the X-ray beam for illumination in normal (N), transverse (T), and flow (F) directions.

8 h at 60°C. Cross sections were microtomed perpendicularly to the plane of the film and studied by AFM technique in the tapping mod in air, at ambient conditions. The AFM images were obtained with a commercial scanning probe microscope (Nanoscope IIIa, Digital Instruments, Santa Barbara, CA) using rectangular type Si probes having a tip radius of about 10 nm, spring constant of 50 Nm^{-1} and resonance frequencies in the 284–362 kHz range.

Usually, a measured HDPE layer thickness was close to the nominal thickness,[21] therefore, the HDPE layers are identified by the nominal layer thickness through the paper.

The only exception was the system with the thinnest HMHDPE layers, of calculated thickness equal to 7 nm, for which the AFM measured thickness was 14 nm.

The multilayered films were delaminated at liquid nitrogen temperature to expose the surface of the HDPE layers. Under these conditions, the layers separated easily without deformation of HDPE surface. The HDPE surface was then investigated with the AFM in a tapping mode.

The crystal structure and texture of multilayered films were studied using wide angle X-ray diffraction (WAXS), small angle X-ray scattering (SAXS), and the X-ray pole figure technique. A WAXS system consisted of a computer controlled wide-angle goniometer associated with pole figure attachment coupled to a sealed-tube source of CuK_α radiation, operating at 30 kV and 30 mA. The CuK_α line was filtered using electronic filtering and the usual thin Ni filter. The slit system that was used for collecting 2Θ scans allowed for the collection of the diffracted beam, with a divergence angle of less than 0.05°. The diffraction reflections from crystals of HDPE orthorhombic crystallographic form from planes parallel to macromolecular chains: (110), (200), (020), and perpendicular to the chains, (002), were analyzed. The reflections from the planes (110) and (200) were recorded in two modes: in transmission and in reflection while at higher 2Θ angles, the reflections from (020) and (002) planes were recorded in the transmission mode. The reflection from (002) plane is the best possible measure of the packing and orientation of chain axes because the normal to this plane coincides with the chain axis in orthorhombic HDPE crystals.

The orientation of crystalline phase of HDPE in the multilayered films was studied by means of X-ray diffraction with pole figures. A WAXS system consisting of a computer-controlled pole figure device associated with a wide-angle goniometer coupled to a sealed tube X-ray generator operating at 30 kV and 30 mA was used in this study. The X-ray beam consisted of Cu K_α radiation filtered electronically and by Ni filter. For pole figure data acquisition we used the procedure elaborated earlier; the details of pole figure determination procedure were described elsewhere.[22] The following diffraction reflections from orthorhombic crystal structure of HDPE were analyzed for the construction of pole figures: (110), (200), (020), and (002). The slit system of the diffractometer was always selected to measure the integral intensity of the appropriate diffraction peak. The necessary corrections for background scattering and sample absorption were introduced to raw data. The pole figure plots were generated by the POD program, a part of the popLA package (Los Alamos National Laboratory, Los Alamos, New Mexico). For every plot the data were normalized to the random distribution density.

Additional measurements of the crystal orientation were performed by using WAXS camera coupled to the X-ray generator (sealed-tube, fine point CuK_α filtered source operating at 50 kV and 35 mA, Philips) using imaging plates for recording the diffraction patterns. The samples were exposed in three orthogonal directions: normal (N), transverse (T), and flow (F), as it is shown in Figure 1. Samples for investigation along the directions N were prepared by sandwiching the film to total thickness of 1 mm, while for the directions T and F (along the film) sandwiches consisting from 25 to 256 pieces (depending on the film thickness) were

prepared, glued together with isocyanate 10 s glue and trimmed to a thickness of 1 mm along T or F direction with a razor blade. Exposed imaging plates (Kodak) were read with PhosphorImager SI system (Molecular Dynamics).

Lamellar orientation was probed by 2-D small angle X-ray scattering (2-D SAXS). The 1.1 m long Kiessig-type vacuum camera was equipped with a capillary collimator (X-Ray Optical Systems Inc.) allowing the resolution of scattering objects up to 40 nm. The camera was coupled to the X-ray generator (sealed-tube, fine point CuK_α Ni filtered source operating at 50 kV and 35 mA, Philips). Exposed imaging plates (Kodak) used as a recording medium were analyzed with PhosphorImager SI system (Molecular Dynamics). The samples were exposed in the N, T, and F directions.

Spherulitic structure of both HDPEs and the multilayered films was studied by a small angle light scattering (SALS) method. The SALS studies utilized He–Ne laser as a light source with the wavelength of 0.6328 μm. The films, submerged in an immersion oil having refractive index of 1.473, were illuminated in the N direction. H_V scattering patterns were recorded photographically. The light intensity distribution versus the scattering angle determined at an azimuthal angle of 45° was used for calculations of an average radius <R>.[23]

DSC thermograms were recorded for samples having mass of about 5 mg during heating at a rate of 10 K/min in a TA Instruments DSC 2920. MDSC measurements were performed during heating at a rate of 2 K/min, amplitude of temperature modulation 0.1 K, and frequency of 1/20 Hz.

RESULTS AND DISCUSSION

2θ diffractograms

The peak intensities from all considered planes depend on both HDPE content and individual HDPE layer thickness. The intensities can be directly compared because for the purpose of X-ray diffraction, the multilayered films were arranged in stacks having the same total thickness. For stacks of films with the same thickness of individual HDPE layers, the peak intensity decreases with the decrease of HDPE content; such comparison requires, however, considering the samples differing also in total thickness prepared at different take off speed in film coextrusion.

The peak intensity from (110) and (200) planes was found at 21.5–21.6° and 23.9–24.0°. Exemplary 2Θ diffractograms recorded in the transmission and reflection modes from (110) and (200) planes are shown in Figures 2 and 3, while those recorded in the transmission mode from (020) and (002) planes are demonstrated in Figures 4 and 5 for both systems studied.

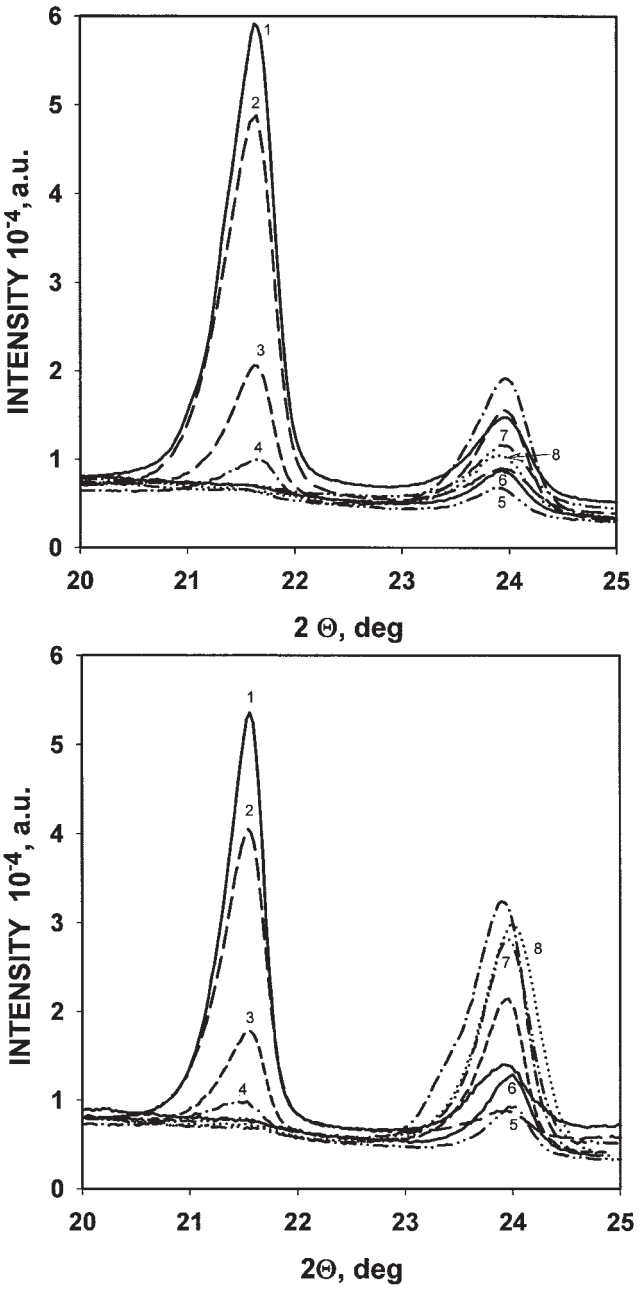

Figure 2 (a) Exemplary 2Θ diffractograms for (110) and (200) planes recorded in reflection mode for LMHDPE control samples and multilayered LMHDPE/PS films: 1 –LMHDPE control (266 μm), 2 –LMHDPE control (40 μm), 3 –LMHDPE50/PS50 (1140 nm), 4 –LMHDPE50/PS50 (190 nm), 5 –LMHDPE10/PS90 (230nm), 6 –LMHDPE10/PS90 (110 nm), 7 –LMHDPE10/PS90(35 nm), 8 –LMHDPE5/PS95 (19 nm). (b). Exemplary 2Θ diffractograms for (110) and (200) planes recorded in reflection mode for HMHDPE control samples and multilayered HMHDPE/PS films: 1 –HMHDPE control (305 μm), 2 –HMHDPE control (51 μm), 3 –HMHDPE50/PS50 (1100 nm), 4 –HMHDPE50/PS50 (180 nm), 5 –HMHDPE10/PS90 (240 nm), 6 –HMHDPE10/PS90 (120 nm), 7 –HMHDPE10/PS90 (40 nm), 8 –HMHDPE5/PS95 (20 nm).

For HDPE control film the peak intensities from (110) and (200) planes recorded both in the reflection and in the transmission modes decrease with the decrease of

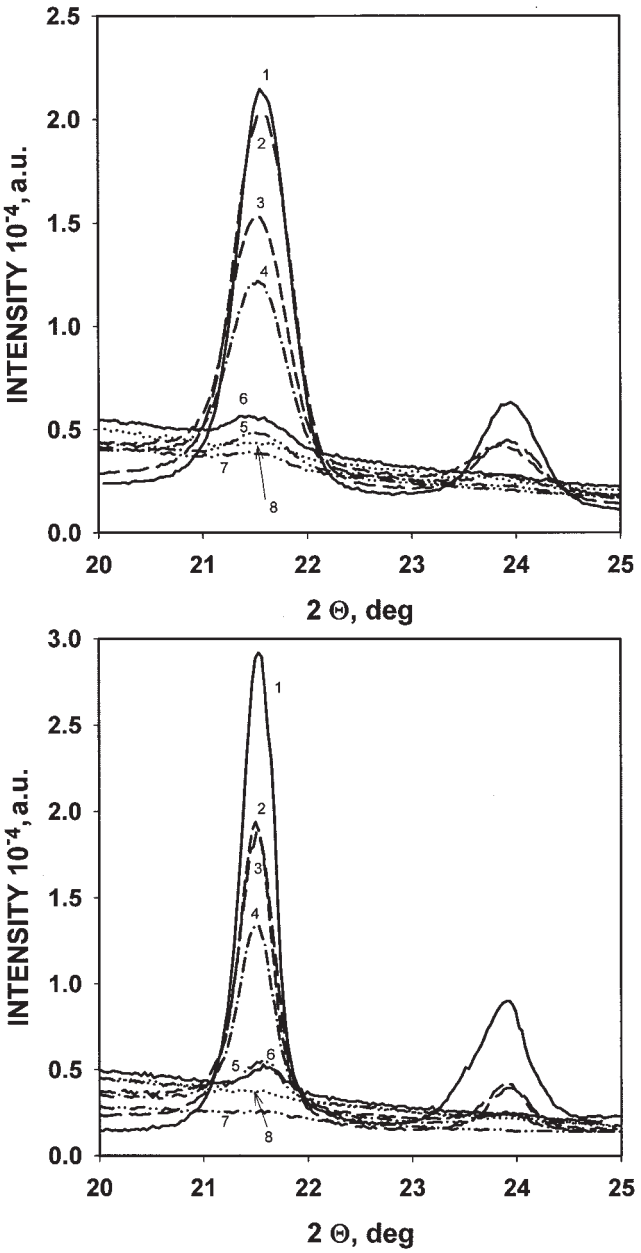

Figure 3 (a) Exemplary 2Θ diffractograms for (110) and (200) planes recorded in transmission mode for LMHDPE control samples and multilayered LMHDPE/PS films: 1 –LMHDPE control (266 μm), 2 –LMHDPE control (40μm), 3 –LMHDPE50/PS50 (1140 nm), 4 –LMHDPE50/PS50 (190 nm), 5 –LMHDPE10/PS90 (230 nm), 6 –LMHDPE10/PS90 (110 nm), 7 –LMHDPE10/PS90(35 nm), 8 –LMHDPE5/PS95 (19 nm).(b) Exemplary 2Θ diffractograms for (110) and (200) planes recorded in transmission mode for HMHDPE control samples and multilayered HMHDPE/PS films: 1 –HMHDPE control (305 μm), 2 –HMHDPE control (51 μm), 3 –HMHDPE50/PS50 (1100 nm), 4 –HMHDPE50/PS50 (180 nm), 5 –HMHDPE10/PS90 (240 nm), 6 –HMHDPE10/PS90 (120 nm), 7 –HMHDPE10/PS90(40 nm), 8 –HMHDPE5/PS95 (20 nm).

thickness of individual film. The peak intensities from (110) planes recorded both in reflection and in transmission and also from (200) planes in the transmission are lower for multilayered films than for HDPE con-

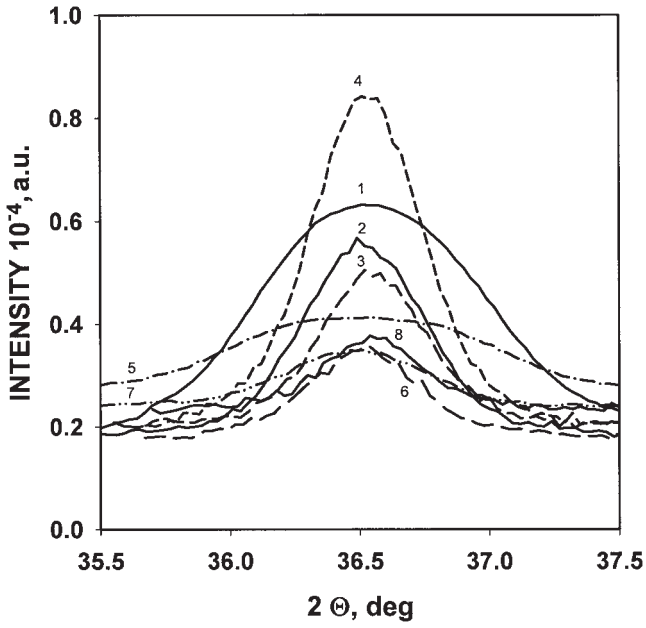

Figure 4 Exemplary 2Θ diffractograms for (020) planes recorded in transmission mode for HDPE control samples and multilayered HDPE/PS films: 1 –LMHDPE control (40 μm), 2 –HMHDPE control (51 μm), 3 –HMHDPE 50/PS50 (1100 nm), 4 –HMHD50/PS50 (180 nm), 5 –LMHDPE90/PS10 (35 nm), 6 –HMHDPE90/PS10 (40 nm), 7 –LMHDPE95/PS5 (19 nm), 8 –HMHDPE95/PS5 (20 nm).

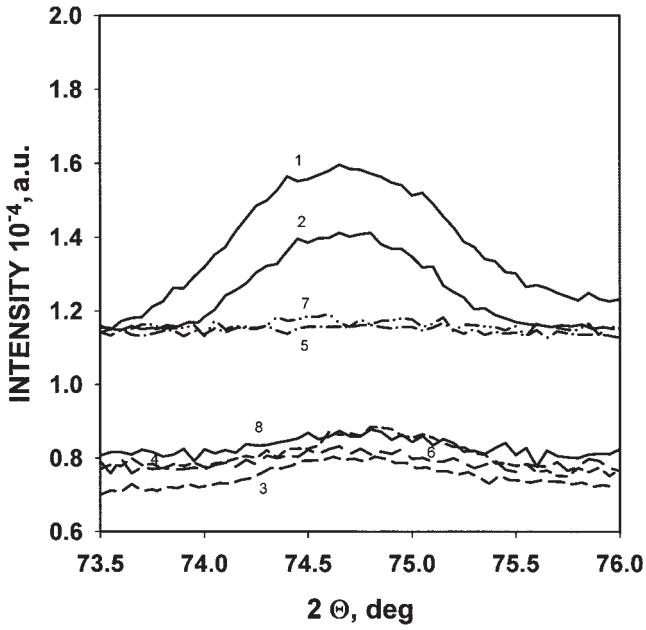

Figure 5 Exemplary 2Θ diffractograms for (002) planes recorded in transmission mode for HDPE control samples and multilayered HDPE/PS films: 1 –LMHDPE control (40 μm), 2 –HMHDPE control (51 μm), 3 –HMHDPE 50/PS50 (1100 nm), 4 –HMHDPE50/PS50(180 nm), 5 –LMHDPE90/PS10 (35 nm), 6 –HMHDPE90/PS10 (40 nm), 7 –LMHDPE95/PS5 (19 nm), 8 –HMHDPE95/PS5 (20 nm).

trol films. For the systems with the same HDPE content, the intensities decrease with the decrease of individual HDPE layer thickness.

Opposite tendencies were found for the peak intensity from (200) planes recorded in the reflection mode. In this case, the intensity is higher for some multilayered systems than for HDPE control films; for the systems with the same HDPE content, it increases with the decrease of individual HDPE layer thickness.

The peaks from planes (020) and (002) in transmission mode are positioned at 36.5° and 74.7°, respectively, for all HDPE control samples (Figs. 4 and 5). The peak intensity values depend on the HDPE content and on individual HDPE layer thickness. However, for the series of samples having the same HDPE content, an increase of the peak intensity with the decrease of HDPE layer thickness is observed.

The intensity analysis of 2Θ scans indicates the orientation of HDPE crystals; in the multilayered systems, it is associated with the decrease of HDPE layer thickness. The decrease of layer thickness enhances the orientation of crystals with (200) planes parallel and (020) and (002) planes normal to the film plane. The peaks from (200) planes recorded in reflection mode have higher intensity for HMHDPE/PS systems than for LMHDPE/PS systems with the same HDPE content and similar individual HDPE layer thickness.

Pole figures

Exemplary pole figures for the HDPE control and a series of multilayered HDPE/PS films are shown in Figures 6–9. For the HDPE control films, the pole figures indicate the presence of preferred orientation of crystals: the pole figures for (200) planes in Figure 6 exhibit maxima at polar regions indicating the preferred orientation of (200) planes mostly normal to the film plane and to FD. The pole figures for (020) planes (in Fig. 7) have high intensity at the equatorial region, the intensity increases with the decrease of thickness of HDPE layers in HDPE control films. The pole figures for (002) planes in Figure 8 exhibit high intensity around its circumference, maximized at polar regions and minimized at equatorial regions; this can result only from a texture component consisting of crystals with (002) planes normal to the film plane with a fraction of crystals with (002) planes normal to FD. The pole figures for (110) planes exhibit minima around polar regions and maxima at the centers.

The orientation of (200) planes in the first texture component of the HDPE control samples enforces the orientation of (020) and (002) planes parallel to FD, while in the second texture component the orientation of (002) plane normal to FD enforces the orientation of planes (002) and (200) parallel to FD. The amplification of intensity at the central part of the (110) pole figure indicates that the significant part of the first texture component are crystals with (002) planes normal to the film plane. Hence, the (020) planes of both populations of crystals have to be parallel to FD as it is clearly seen in the respective pole figures in Figure 7.

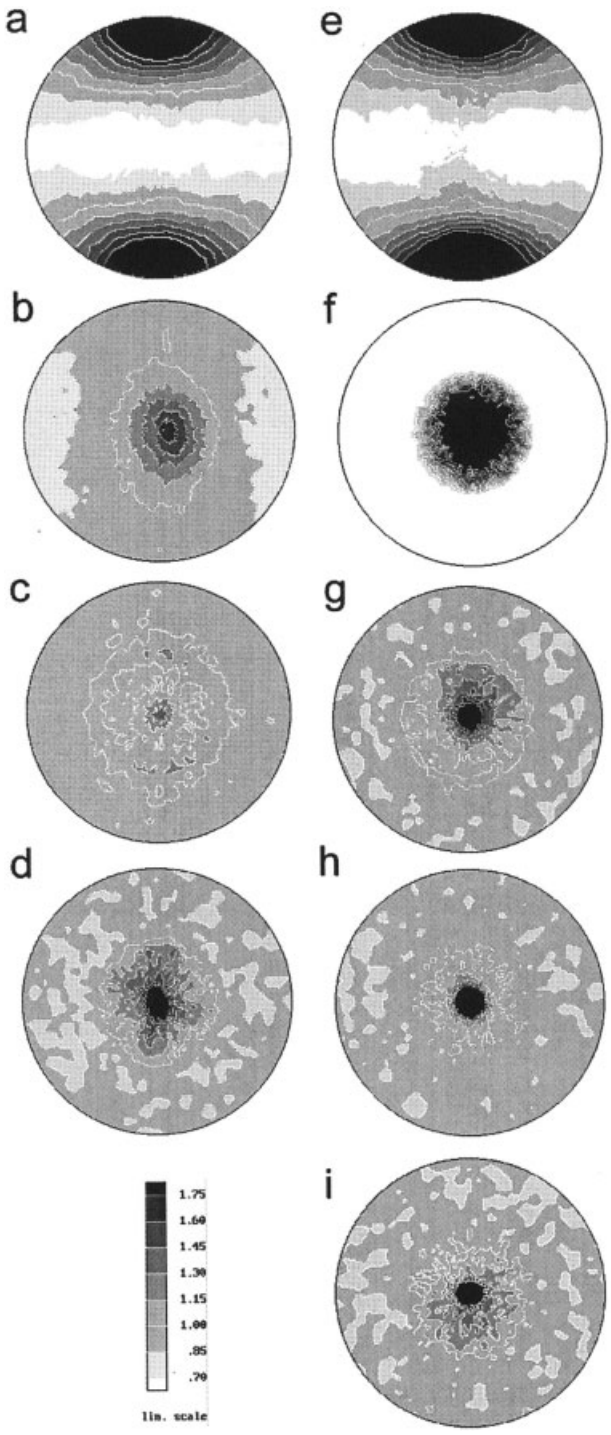

Figure 6 Exemplary pole figures for HDPE control samples and multilayered HDPE/PS films for (200) planes: (a) LMHDPE control (40 μm), (b) LMHDPE70/PS30 (1530 nm), (c) LMHDPE10/PS90(110 nm), (d) LMHDPE5/PS95 (19 nm), (e) HMHDPE control (51 μm), (f) HMHDPE50/PS50 (1100 nm), (g) HMHDPE10/PS90 (120 nm), (h) HMHDPE5/PS95 (20 nm), (i) HMHDPE5/PS95 (7 nm). F direction vertical.

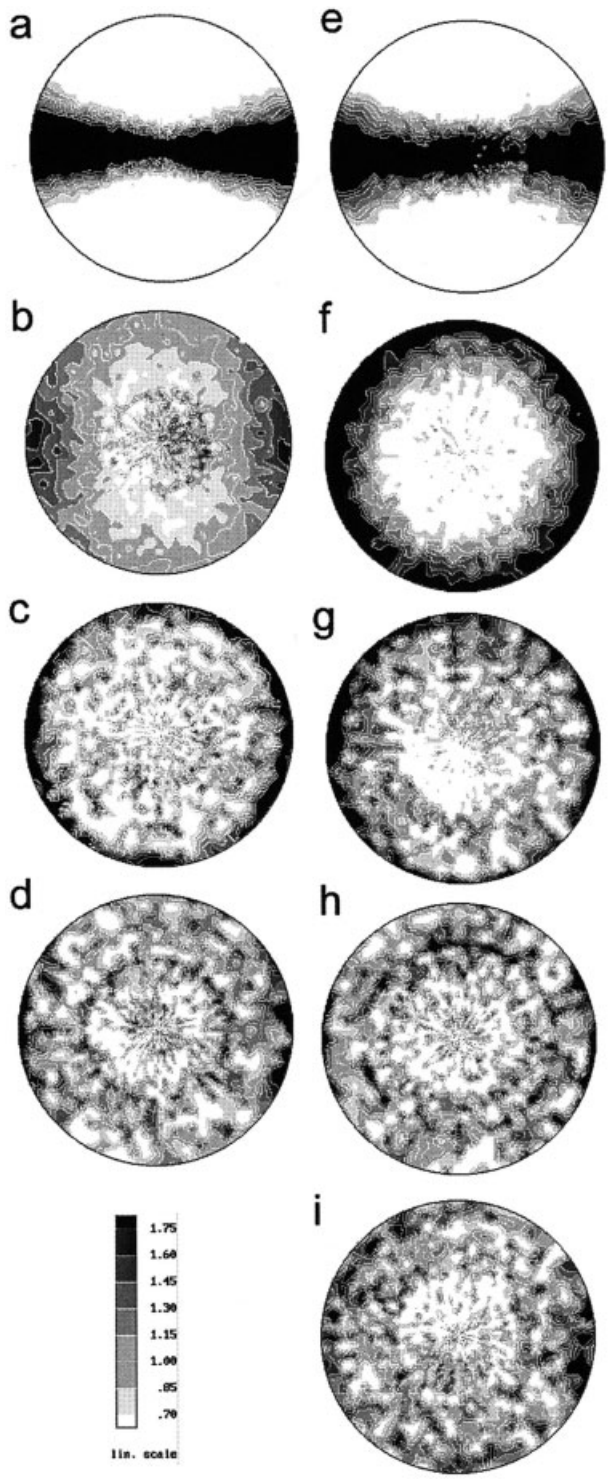

Figure 7 Exemplary pole figures for HDPE control samples and multilayered HDPE/PS films for (020) planes: (a) LMHDPE control (40 μm), (b) LMHDPE70/PS30 (1530 nm), (c) LMHDPE10/PS90 (110 nm), (d) LMHDPE5/PS95 (19 nm), (e) HMHDPE control (51 μm), (f) HMHDPE50/PS50 (1100 nm), (g) HMHDPE10/PS90 (120 nm), (h) HMHDPE5/PS95 (20 nm), (i) HMHDPE5/PS95 (7 nm). F direction vertical.

The extrusion and the take-up processes enforce some orientation of HDPE molten film that is reflected in preferred orientation of crystals during solidification. However, if HDPE is layered between PS layers, its texture is significantly different than in HDPE control film, which is clearly visible in pole figures for multilayered systems.

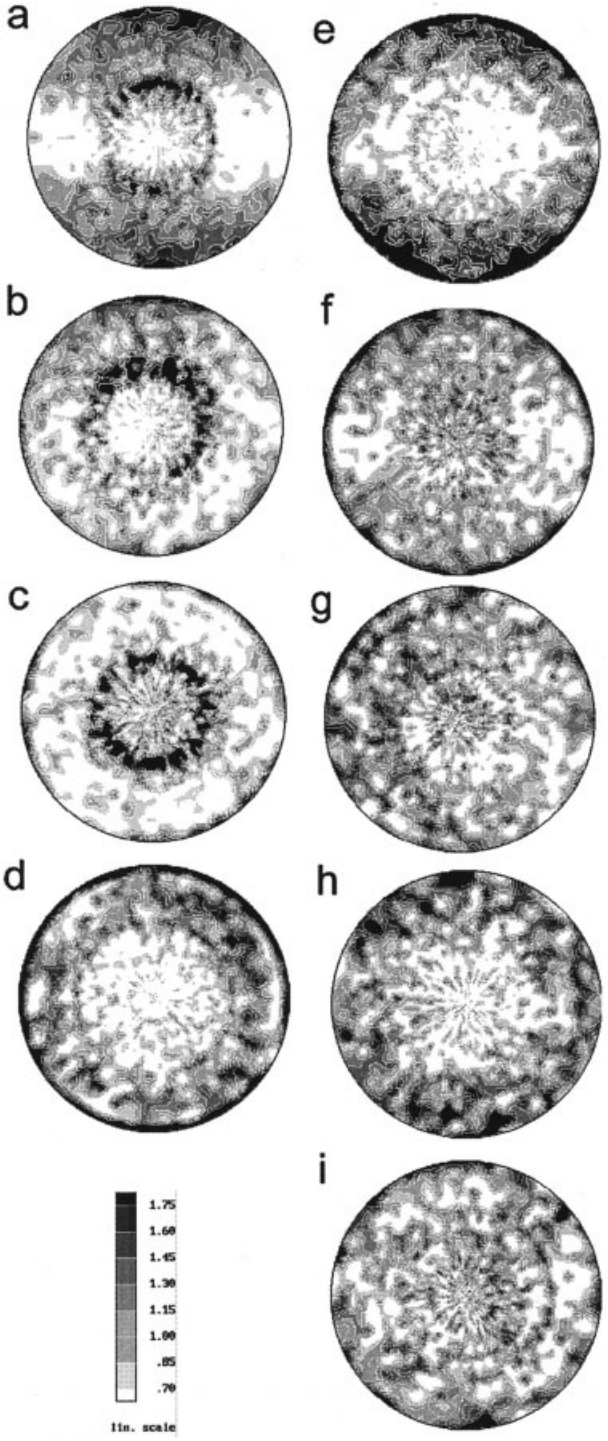

Figure 8 Exemplary pole figures for HDPE control samples and multilayered HDPE/PS films for (002) planes: (a) LMHDPE control (40 μm), (b) LMHDPE70/PS30 (1530 nm), (c) LMHDPE10/PS90 (110 nm), (d) LMHDPE5/PS95 (19 nm), (e) HMHDPE control (51 μm), (f) HMHDPE50/PS50 (1100 nm), (g) HMHDPE10/PS90 (120 nm), (h) HMHDPE5/PS95 (20 nm), (i) HMHDPE5/PS95 (7 nm). F direction vertical.

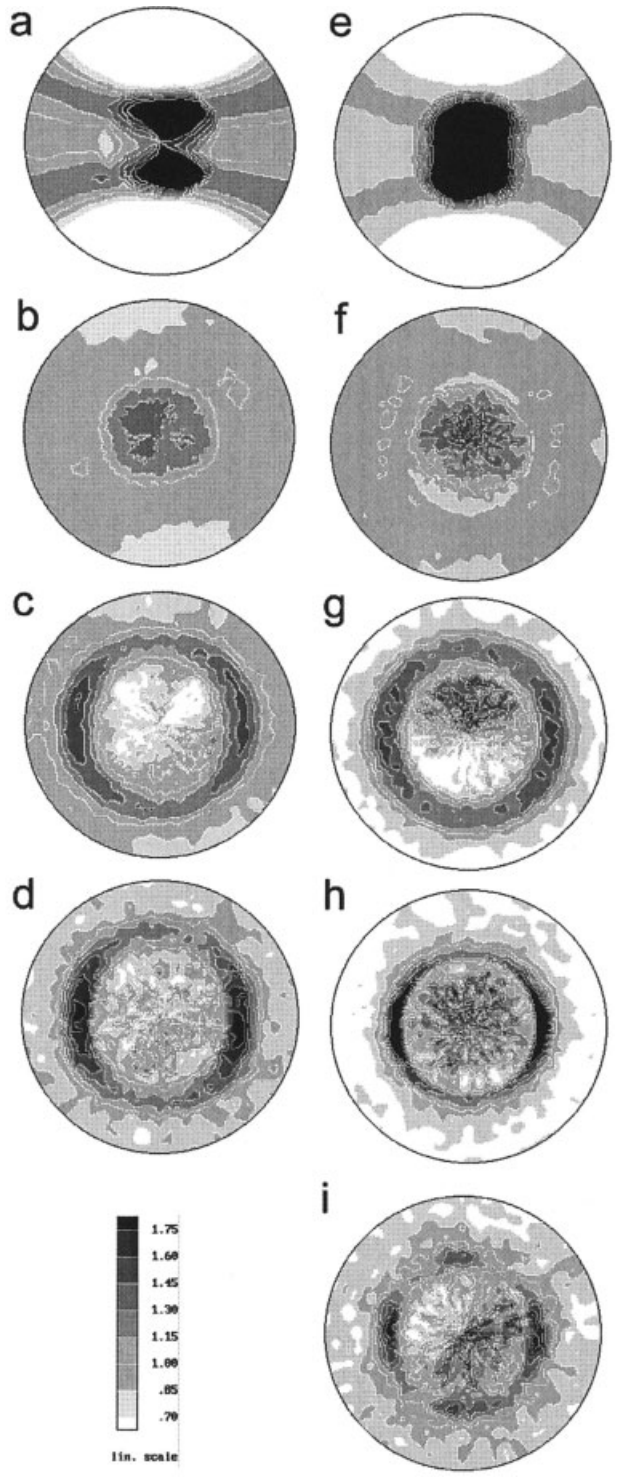

Figure 9 Exemplary pole figures for HDPE control samples and multilayered HDPE/PS films for (110) planes: (a) LMHDPE control (40 μm), (b) LMHDPE70/PS30 (1530 nm), (c) LMHDPE10/PS90(110 nm), (d) LMHDPE5/PS95 (19 nm), (e) HMHDPE control (51 μm), (f) HMHDPE50/PS50 (1100 nm), (g) HMHDPE10/PS90 (120 nm), (h) HMHDPE5/PS95 (20 nm), (i) HMHDPE5/PS95 (7 nm). F direction vertical.

For the multilayered systems, the intensity at the centers of the pole figures for (200) planes (Fig. 6) increases in comparison to that for the HDPE control films. As the individual HDPE layer gets thinner, the concentration of normals to (200) planes becomes even stronger reflecting the increasing orientation of (200) planes in the film plane.

The pole figures for (020) planes for the multilayered samples (Fig. 7) exhibit the minima around centers and the maxima around the circumferences. This indicates the orientation of (020) planes normal to the film plane. Amplification of the intensity near the equator, better visible for the systems of LMHDPE/PS, reflects some orientation of (200) planes parallel to FD. The intensity in the pole figures for (002) planes increases with the increase of α angle. Apparently the preferred orientation of (200) planes parallel and of (020) planes perpendicular to the film plane results from the interaction of HDPE with the interface with PS during solidification while some orientation of (020) planes parallel to FD in the systems of LMHDPE/PS results from the difference between the film take-up rate by the chill-roll and the film extrusion rate.

The pole figures for (110) planes for multilayered samples shown in Figure 9 for the thickest HDPE layers have the maxima at the centers. With the decrease of the HDPE layer thickness, the highest intensity concentrates at the angle α equal approximately 60–70°. Further decrease of HDPE layer thickness results in the clustering of (110) normals in two arcs crossing the equator. The latter effect results from the concentration of (110) planes inclined to the film plane at the angle of 60–70° and at 20–30° to the F direction.

For series of films with the same total thickness the orientation increases with the decrease of HDPE individual layer thickness.

Two dimensional diffraction patterns

The exemplary two dimensional diffraction patterns recorded for multilayered films containing LMHDPE illuminated in N, T, and F directions are shown in Figure 10, The patterns were scanned in the vertical and horizontal positions to obtain a more precise information about the reflection intensities. On all patterns, the reflections from planes (110) and (200) are clearly discernible. While the (020) reflections can also be detected on a 2D- pattern ($2\Theta = 36.5°$), (002) reflection cannot be seen on a 2D-pattern since 2Θ is around 75° for (002) reflection. Here, the two dimensional diffraction patterns serve as a means for the verification of the pole figures correctness. The signal recorded on each pattern originates from crystallographic planes inclined at the Θ angle to the beam (Θ being around 11° for (110) planes and around 12° for (200) planes). Thus, the ND pattern reflects the orientation of crystals nearly normal to the film plane, which is visible in pole figures for α near 90°. The TD and FD patterns reflect the orientation of the planes

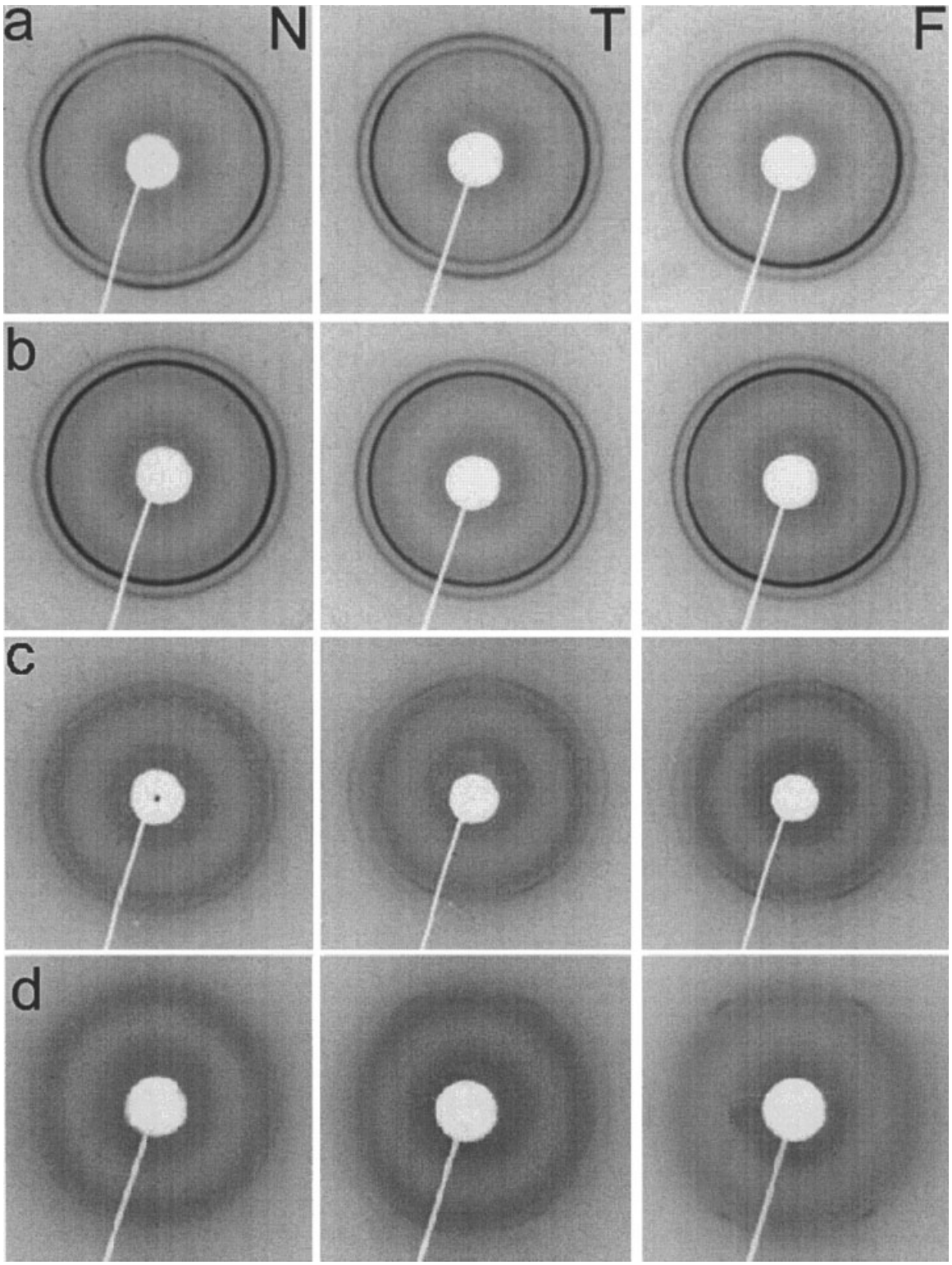

Figure 10 Exemplary 2D diffraction patterns recorded in ND, TD, and FD for: (a) LMHDPE control (40 μm), (b) LMHDPE70/PS30 (1530 nm), (c) LMHDPE10/PS90 (110 nm), (d) LMHDPE5/PS95 (19 nm).

oriented along the vertical axis and along the equator of a corresponding pole figure. The strong signals at polar and equatorial regions of those patterns originate from planes parallel and normal to the equatorial plane, respectively.

For the LMHDPE control samples, only a weak orientation is visible on FD patterns, while on the ND and TD patterns the orientation is more pronounced as it is seen in Figure 10. On the ND patterns more intense reflections from (200) planes are visible at po-

lar regions, while the strongest reflections from (110) planes are located on arcs crossing the equator. These tendencies are enhanced by the decrease of the film thickness; they are clearly visible for the thinner films while rather poorly for the thickest, 266 μm thick film. The observed features are in agreement with the pole figures constructed for (110) and (200) planes.

In the diffractions patterns for the multilayered systems with LMHDPE in N direction the signal from (200) plane is slightly stronger in the polar than in the equatorial regions. The signal becomes hardly discernible with the decrease of HDPE layer thickness. Thus, in thicker HDPE layers, the population of (200) planes normal to the film plane exhibits some orientation in the direction perpendicular to FD. The reflections from (110) planes are stronger in the equatorial than in the polar regions of the diffraction patterns. These observations agree well with the respective pole figures in Figures 6 and 9.

The diffraction patterns in the FD and TD are similar. The reflections from (200) planes are the strongest at the equatorial regions, which indicates the orientation of most of (200) planes parallel to the film plane. With the decrease of HDPE layer thickness, the signal from (200) planes becomes hardly visible in equatorial regions of those patterns. The signal from (110) planes is intense on the arcs with two maxima formed on each arc at 30° and –30° with respect to the vertical line. The stronger signals from (110) planes in FD than in TD indicates the orientation of crystals with (002) planes normal to the film plane and FD. The weaker signals from (110) from (110) planes in TD are due to a small fraction of crystals with (002) planes normal to the film plane and parallel to FD.

Similar tendencies were found on 2D diffraction patterns shown in ref. 21 for the systems containing HMHDPE.

Small angle X-ray scattering

The SAXS patterns for the HDPE control and multilayered samples are demonstrated in Figures 11 and 12. SAXS patterns recorded for control samples of both HDPEs in ND and TD are asymmetrical; they are elongated in the vertical direction; the intensity on these patterns is higher at polar than at equatorial regions. The asymmetry of these SAXS patterns indicates a slight orientation of lamellae in the direction perpendicular to FD. The equatorial signals in ND and TD and the entire pattern recorded in FD originate from the lamellae population parallel to FD, but differently oriented with respect to the film plane. The stronger signal at the polar regions of ND and TD patterns indicate the population of lamella normal to the film plane and to FD. These populations of lamellae correspond to the first and the second component of the crystal texture detected by WAXS, respectively. The decrease of film thickness results in the amplification of these tendencies (see Figs. 11 and 12).

The long period measured for LMHDPE control thick films equals approx. 19–20 nm with the exception of the second crystal population in the thinnest film, for which the long period is equal to 17 nm. The long period measured for HMHDPE control equals 26–27 nm for 305 μm thick film, and slightly less, 25 nm for 51 μm thick film. In both polyethylenes, with the decrease of film thickness the long period becomes hardly detected in the equatorial regions of TD and FD patterns indicating the decrease of lamellae population parallel to the film plane.

The SAXS patterns recorded for the multilayered systems exhibit also deviation from a symmetric shape (see Figs. 11 and 12). The ND patterns are somewhat elongated in the vertical direction but less than the respective patterns for the HDPE control samples. The long period for HDPE component can be easily detected from the intensity at the polar regions for all samples. With the decrease of HDPE layer thickness, the intensity at the equatorial regions diminishes with respect to that at the polar regions and for the thinnest HDPE layers the long period becomes hard to detect. The FD and TD patterns are strong and significantly elongated in the vertical direction. These strong streaks in SAXS patterns indicate the presence of gaps between LMHDPE and PS layers. In those patterns, the intensity is higher at the equatorial than at the polar regions. While the long period can be detected at the polar regions, it is difficult or even impossible to identify long period at the equatorial regions because of a strong scattering that resulted from incomplete fusion of HDPE and PS layers. The polar intensity of ND patterns is similar to the equatorial intensity of TD patterns and the polar intensity of TD patterns is similar to the equatorial intensity in ND patterns. Also, the equatorial intensity of ND patterns is close to the polar intensity of FD patterns. The intensity in ND patterns for the multilayered systems and in the polar regions of the other patterns is primarily controlled by the HDPE content and diminishes with its decrease. For the samples with the thinnest HDPE layers, the polar region intensity is the lowest and goes below that in other systems having the same HDPE content but larger HDPE layer thickness. The equatorial intensities of TD and FD patterns are at a similar high level for all samples studied.

It follows from the earlier mentioned that the lamellae are predominantly normal to the film plane, with the long period of roughly 20 and 26 nm for LMHDPE and HMHDPE, respectively. With the decrease of the

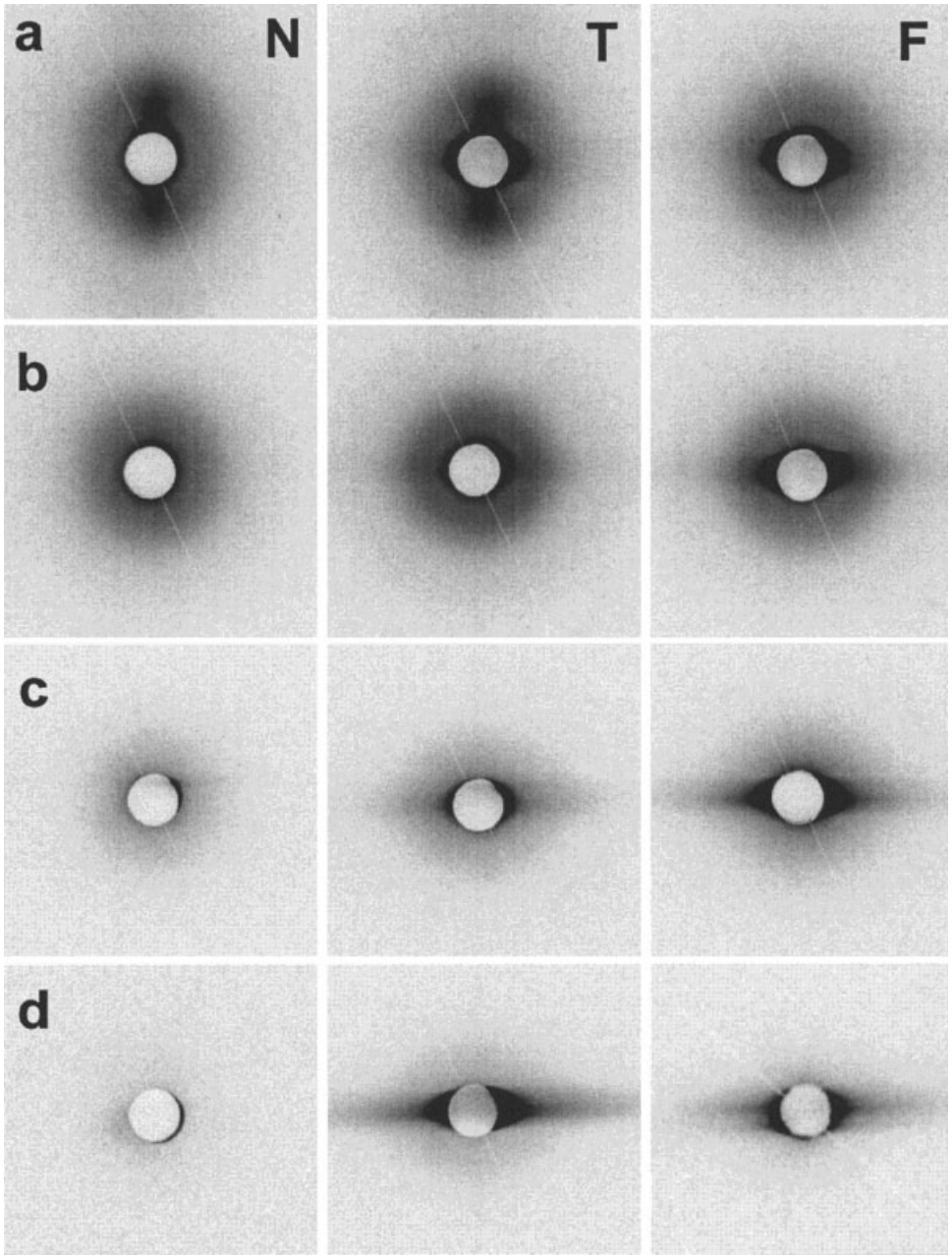

Figure 11 Exemplary SAXS patterns recorded in ND, TD, and FD for: (a) LMHDPE control (40 μm), (b) LMHDPE70/PS30 (1530 nm), (c) LMHDPE10/PS90 (110 nm), (d) LMHDPE5/PS95 (19 nm).

HDPE layer thickness, the edge-on orientation of lamellae prevails.

Small angle light scattering

Exemplary H_V patterns recorded for the systems studied are shown in Figure 13. Typical four-leaf patterns point out the presence of spherulites in both HDPEs, having diameter about 7 μm in HMHDPE and slightly larger, about 8 μm in LMHDPE. Similar patterns obtained for the multilayered systems indicate a spherulitic type of crystalline phase organization in the confined HDPE layers. Spherulite diameter increases to about 12 μm in HMHDPE layers and to 9 μm in LMHDPE layers.

This type of structure is preserved in both LMHDPE and HMHDPE layers of thickness above 100 nm. As the individual HDPE layer thickness decreases below 100 nm, the spherulitic type of crystalline phase organization vanishes.

AFM

AFM studies of surfaces of LMHDPE layers revealed spherulitic structure, with twisted lamellae

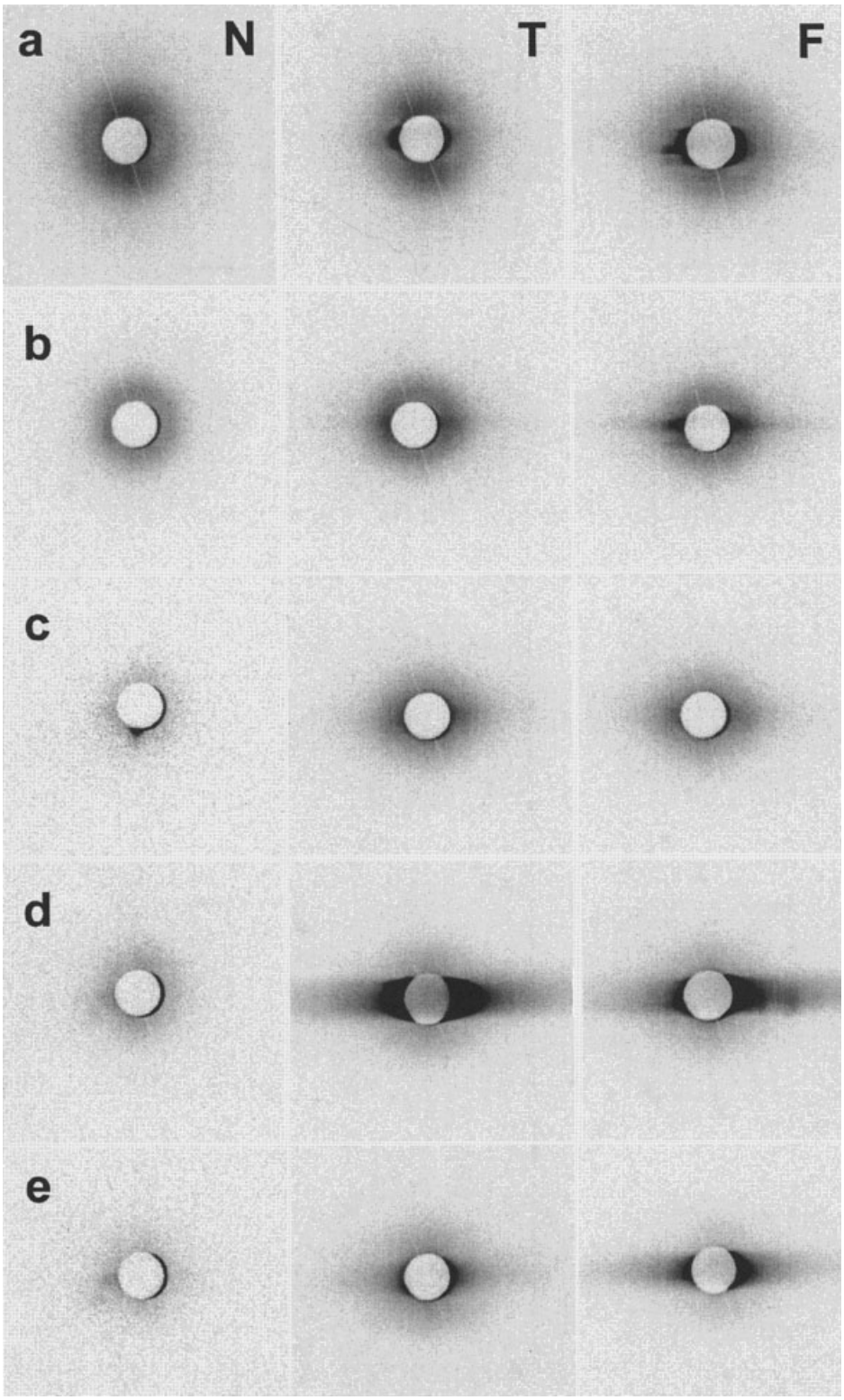

Figure 12 Exemplary SAXS patterns recorded in ND, TD, and FD for: (a) HMHDPE control (51 μm), (b) HMHDPE50/PS50 (1100 nm), (c) HMHDPE10/PS90 (120 nm), (d) HMHDPE5/PS95 (20 nm), (e) HMHDPE5/PS95 (7 nm).

preserved still in 220 nm thick LMHDPE layers, as it is shown in Figure 14(a). In 35 nm thick LMHDPE layers, the edge-on lamellae several micrometers long are visible [Fig. 14(b)] They are no longer twisted as in the thicker layer (1890 nm thick), shown in Figure 3(c). No preferred orientation of those lamellae with respect to FD was found.

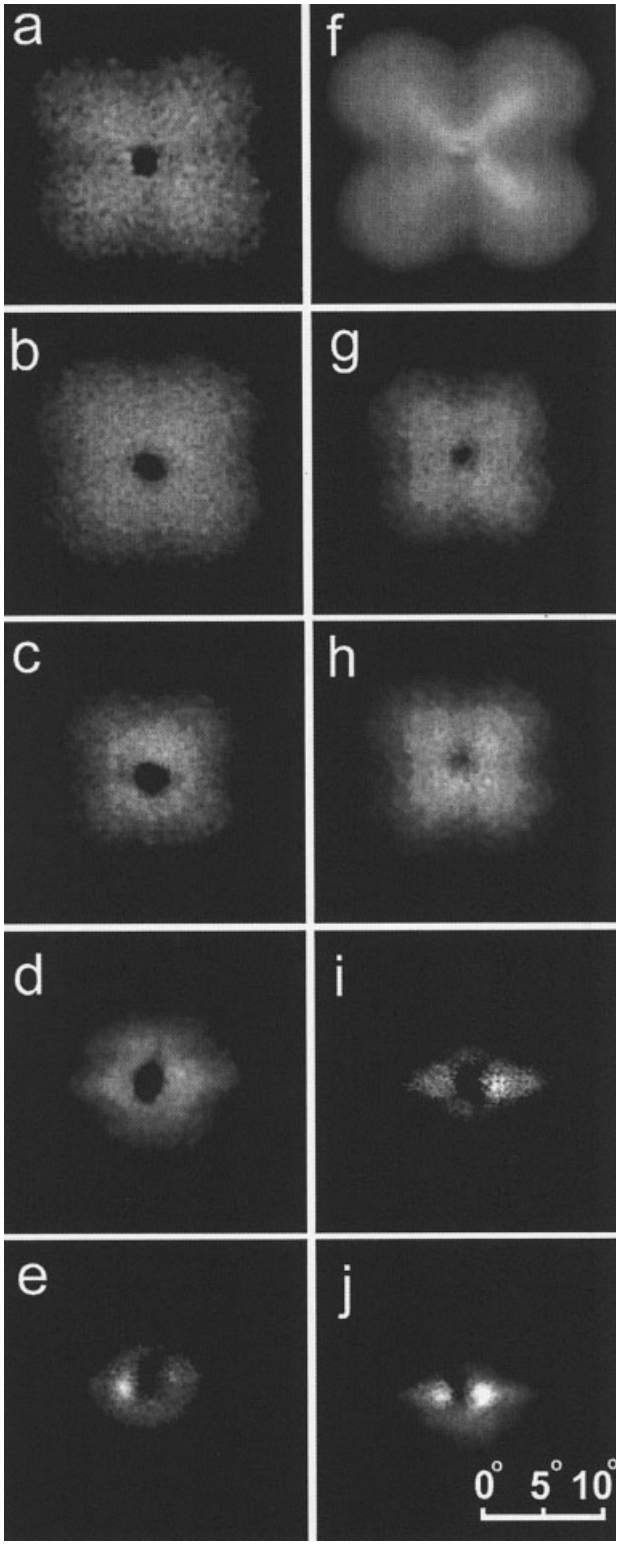

Figure 13 Exemplary SALS H_V patterns recorded in ND for: (a) LMHDPE (137 μm), (b)-LMHDPE10/PS90 (230 nm), (c) LMHDPE10/PS90 (110 nm), (d) LMHDPE10/PS90 (35 nm), (e) LMHDPE5/PS95 (19 nm), (f) HMHDPE (51 μm), (g) HMHDPE10/PS90 (240 nm), (h) HMHDPE10/PS90 (120 nm), (i) HMHDPE10/PS90 (30 nm), (j) HMHDPE5/PS95 (7 nm).

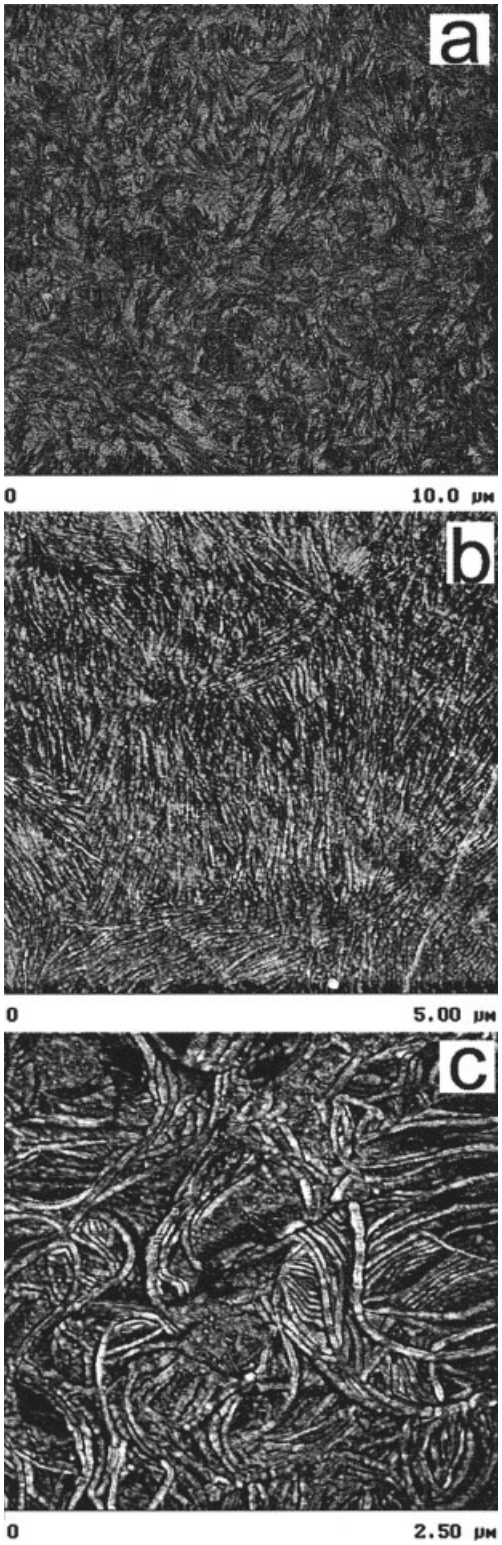

Figure 14 AFM images of peeled surfaces of LMHDPE layers in LMHDPE/PS multilayered films: (a) LMHDPE20/PS80 (220 nm), (b) LMHDPE10/PS90 (35 nm), (c) LMHDPE90/PS10 (1890 nm).

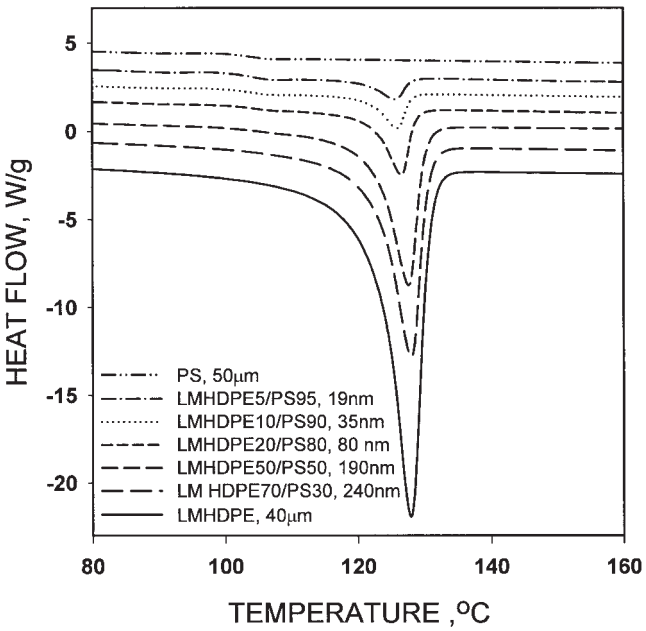

Figure 15 DSC heating thermograms of LMHDPE control and LMHDPE/PS films recorded at a heating rate of 10 K/min.

DSC

Figure 15 demonstrates DSC heating thermograms of LMHDPE/PS multilayered systems recorded at a heating rate of 10 K/min. The melting temperature decreases from 128.0°C for LMHDPE control and LMHDPE 70/PS 30 (240 nm) to 125.7°C for the system with the thinnest 19 nm thick layers of LMHDPE. Also, the melting enthalpy of LMHDPE decreases with the decrease of LMHDPE layer thickness. Crystallinity level of HDPE, calculated assuming the enthalpy of melting of PE crystalline phase of 293 J/g, changes from 56 wt % from LMHDPE control, through 50 wt % for 240 nm thick layers in LMHDPE 70/PS30 to 40 wt % for the 19 nm thick layers in LMHDPE5/PS95.

Figures 16 and 17 show exemplary MDCS scans for both LMHDPE/PS and HMHDPE/PS multilayered systems and control polyethylene films. The temperature of endothermic peaks of nonreversing signal decreases with the decrease of thickness of individual HDPE layers from 127.2°C for LMHDPE control to 126.1°C for the systems with 19 nm thick LMHDPE layers. For HMHDPE systems, the respective temperatures are 131.3 and 129.9°C. Reversing signal for HDPE control films exhibit broad peak at the temperature lower by 0.6°C, than that of nonreversing signal peak. With the decrease of individual HDPE layer thickness the peak becomes even broader but as the HDPE layer thickness decreases beyond 100 nm it sharpens and its temperature decreases, more than the temperature of nonreversing signal peak. For the systems with the 19 nm thick LMHDPE layers, the difference between positions of both peaks is about 2°C; for the systems with HMHDPE layers 20 nm thick it also differs by 2°C and by 2.5°C for 7 nm thick HMHDPE layers, respectively. The proportion between reversing and nonreversing heat flow peaks change; with the decrease of the HDPE individual layer thickness the reversing signal peak increases.

CONCLUSIONS

The morphology of HDPE in the systems studied is greatly affected by the presence of HDPE/PS interfaces. The changes in orientation of crystallographic planes as well as in orientation of lamellae because of the presence of interfaces were detected. In this aspect both HDPEs behave very similar independently of their different molecular weight.

In the control HDPE samples, the two fractions of lamellae are found: the lamellae normal to the film plane and normal to FD (with (002) planes normal to FD) and the lamellae parallel to FD predominantly oriented normal to the film plane (with (200) planes normal to FD).

In the HDPE layers confined between PS layers, we observed the texture composed of lamellae normal to the interface with (200) crystallographic planes paral-

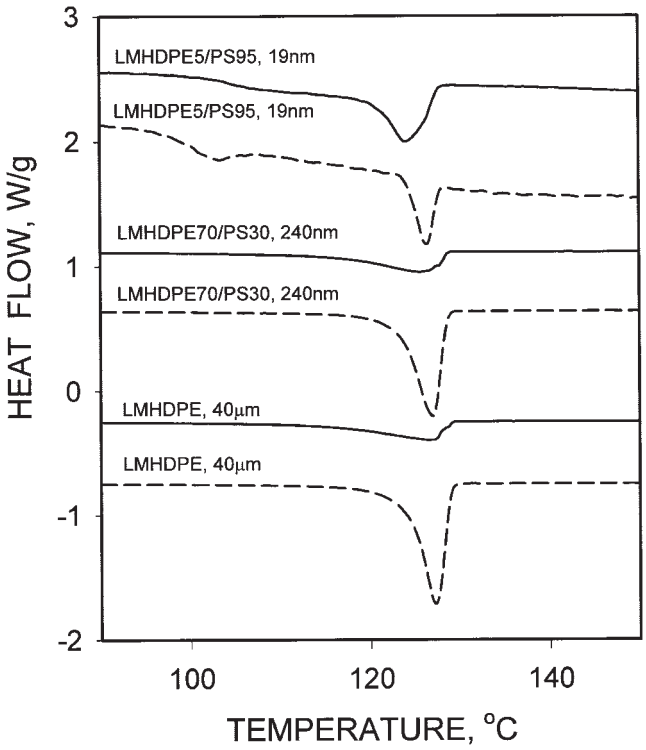

Figure 16 MDSC heating thermograms of LMHDPE control and LMHDPE/PS films: reversing heat flow, solid line, nonreversing heat flow, dashed line. For multilayered films heat flow scaled to LMHDPE content.

lel to the interface. In LMHDPE, some orientation of crystals with planes (002) normal and (020) parallel to FD direction was found. Thus, the HDPE macromolecule fragments, which form crystals, are parallel to the interface between both polymers. The preferred orientation of (200) planes begins to show up in rather thick layers of HDPE that are not severely spatially confined. We attribute this effect to the presence of thin interfacial layer of HDPE having strong orientation of crystals with (200) planes parallel to the interface with PS. With the decrease of HDPE layer thickness, the central unaffected part of HDPE layers becomes thinner and the parts affected by the interface play now more significant role.

SALS patterns and AFM studies demonstrate that spherulitic structure is preserved in HDPE layers thicker than 100 nm. Since the diameter of those aggregates change only slightly with the many folds decrease of individual HDPE layer thickness, the bulk spherulites in thick HDPE layers become discoids in thin layers. In the HDPE layers thinner than 100 nm, bundles of edge-on lamellae are found. The orientation of lamella with respect to the film plane, with (200) planes in the film plane and (020) planes normal to the film plane, is schematically drawn in Figure 18.

Comparison of intensity of (200) peaks recorded in reflection mode indicates, however, stronger crystal orientation in HMHDPE.

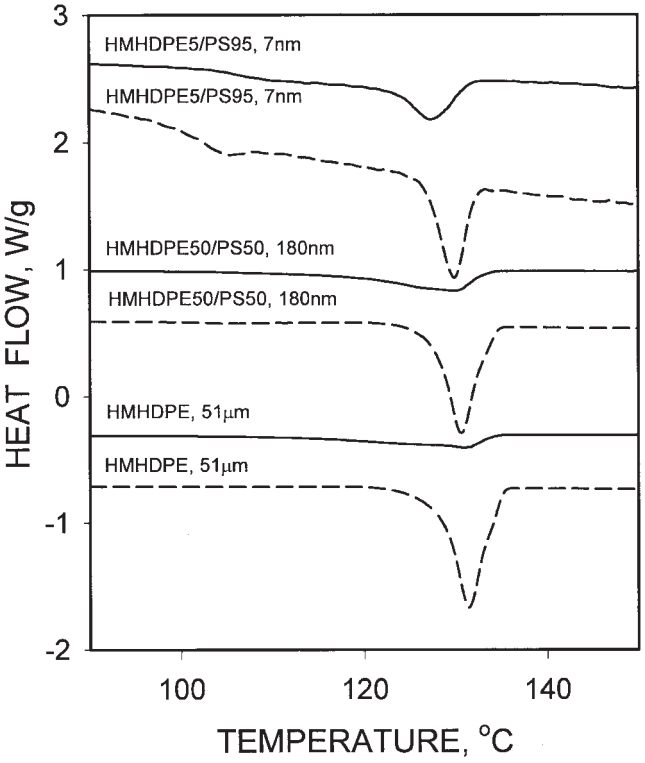

Figure 17 MDSC heating thermograms of HMHDPE control and HMHDPE/PS films: reversing heat flow, solid line, nonreversing heat flow, dashed line. For multilayered films heat flow scaled to HMHDPE content.

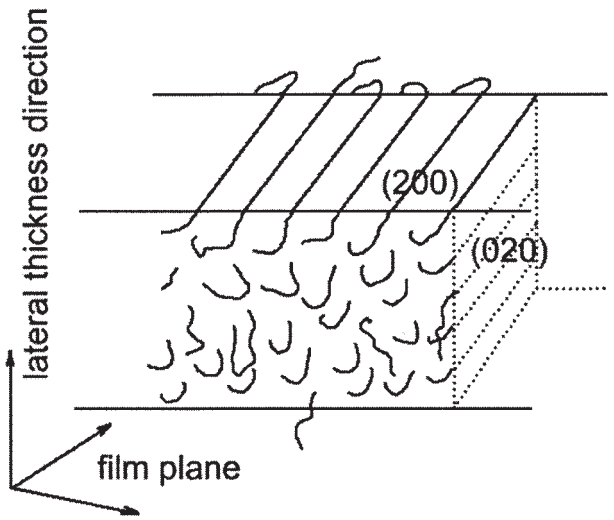

Figure 18 The orientation of lamellae in nanolayers with respect to the film plane.

The fraction of lamellae parallel to the interface detected by SAXS in thicker HDPE layers disappears with the thinning of the layers. The conclusion drawn based on X-ray studies is supported by AFM images of HDPE layers where only edge-on straight lamella were found on the surface of delaminated HDPE layer for LMHDPE/PS system, similarly as it was observed previously for HMHDPE/PS.[21]

No significant shift in X-ray diffraction peak positions was found because of decreased HDPE layer thickness, unlike in the isotactic polypropylene/PS systems studied by Jin et al.[19]

However, the thinnest HDPE layers exhibit the decreased periodicity of the structure, which most probably should be correlated with the lower perfection of crystals due to spatial confinement. DSC results demonstrate the decrease of melting temperature of crystals and the crystallinity level with thinning of HDPE layers. Since similar long period was determined for the multilayered films based on the same HDPE, nearly independently of the individual layer thickness, the decrease of crystallinity also indicates the decrease of lamellae thickness.

The results show that with thinning of individual HDPE layers the reorganization phenomena during heating occur at lower temperature and are more intense, which is also suggestive for a decreased perfection of crystals formed in constrained space.

References

1. Muratoglu, O. K.; Argon, A. S.; Cohen, R. E. Polymer 1995, 36, 2143.
2. Abe, H.; Kikkawa, Y.; Iwata T.; Aoki, H.; Akehata, T.; Doi, Y. Polymer 2000, 41, 867.
3. Padden, F. J., Jr.; Keith, H. D. J Appl Phys 1966, 37, 40.

4. Tsuji, M.; Novillo, F. A.; Fujita, M.; Murakami, S.; Kohjiya, S. J Mater Res 1999, 14, 251.
5. Sakai, Y.; Imai, M.; Kaji, K.; Tsuji, M. J Crystal Growth 1999, 203, 244.
6. Cho, K. W.; Kim, D. W.; Yoon, S. Macromolecules 2003, 36, 7652.
7. Bogdanov, B.; Vidts, A.; Schacht, E.; Berghmans, H. Macromolecules 1999, 32, 726.
8. Ryan, A. J.; Hamley, I. W.; Bras, W.; Bates, F. S. Macromolecules 1995, 28, 3860.
9. Rangarajan, P.; Register, R. A.; Adamson, D. H.; Fetters, L. J.; Bras, W.; Naylor, S.; Ryan, A. J. Macromolecules 1995, 28, 1422.
10. Quiram, D. J; Register, R. A.; Marchand, G. R. Macromolecules 1997, 30, 4551.
11. Hamley, I. W.; Fairclough, J. P. A.; Bates, F. S.; Ryan, A. J. Polymer 1998, 39, 1429.
12. Nojima, S.; Tanaka, H.; Rohadi, A.; Sasaki, S. Polymer 1998, 39, 1727.
13. Loo, Y.L.; Register, R. A.; Ryan, A. J.; Dee, G. T. Macromolecules 2001, 34, 8968.
14. Xu, J.T.; Fairclough, J. P. A.; Mai, S.M.; Ryan, A. J. J Mater Chem 2003, 13, 2740.
15. Zhu, L.; Cheng, S. Z. D.; Huang, P.; Ge, Q.; Quirk, R. P.; Thomas, E. L.; Lotz, B.; Hsiao, B. S.; Yeh, F.; Liu, L.-Z. Adv Mater 2002, 14, 31.
16. Baer, E.; Hiltner, A.; Keith, H. D. Science 1987, 235, 1015.
17. Kerns, J.; Hsieh, A.; Hiltner, A.; Baer, E. J Appl Polym Sci 2000, 77, 1545.
18. Mueller, C.; Topolkaraev, V.; Soerens, D.; Hiltner, A.; Baer, E. J Appl Polym Sci 2000, 78, 816.
19. Jin, Y.; Rogunova, M.; Hiltner, A.; Baer, E.; Nowacki, R.; Galeski, A.; Piorkowska, E. J Polym Sci Part B: Polym Phys 2004, 42, 3380.
20. Pan, S. J.; Im, J.; Hill, M. J.; Keller, A.; Hiltner, A.; Baer, E. J Polym Sci Part B: Polym Phys 1990, 28, 1105.
21. Bernal-Lara, T. E.; Liu, R.Y. F.; Hiltner, A.; Baer, E. Polymer 2005, 46, 3043.
22. Galeski, A.; Bartczak, Z.; Argon, A. S.; Cohen, R. E. Macromolecules 1992, 25, 5705.
23. Bartczak, Z.; Galeski, A. Polymer 1990, 31, 2027.